Letter

Flocking with random nonreciprocal interactions

Jiwon Choi [1], Jae Dong Noh [2], and Heiko Rieger [1,*]
[1]Department of Physics & Center for Biophysics, Saarland University, Campus E2 6, 66123 Saarbrücken, Germany
[2]Department of Physics, University of Seoul, Seoul 02504, South Korea

(Received 26 June 2025; accepted 1 November 2025; published 11 December 2025)

Flocking is ubiquitous in nature and emerges due to short- or long-range alignment interactions among self-propelled agents. Two unfriendly species that antialign or even interact nonreciprocally show more complex collective phenomena, ranging from parallel and antiparallel flocking over run-and-chase behavior to chiral phases. Whether flocking or any of these collective phenomena can survive in the presence of a large number of species with random nonreciprocal interactions remained elusive so far. As a first step here, the extreme case of a Vicsek-like model with fully random nonreciprocal interactions between the individual particles is considered. For infinite-range interaction, as soon as the alignment bias is of the same order as the random interactions, the ordered flocking phase occurs, but deep within this phase, the random nonreciprocal interactions can still support global chiral and oscillating states in which the collective movement direction rotates or oscillates slowly. For short-range interactions, moreover, even without alignment bias self-organized cliques emerge, in which medium-size clusters of particles that have predominantly aligning interactions meet accidentally and stay together for macroscopic times. These results may serve as a starting point for the study of multispecies flocking models with nonrandom but complex nonreciprocal interspecies interactions.

DOI: 10.1103/y26b-qfym

Introduction. Active matter consists of particles that consume energy to use it as a fuel for movement, force generation, deformation, or proliferation [1–4] and gives rise to collective phenomena that are absent in equilibrium systems, like flocking [5], motility-induced phase separation [6], spontaneously flowing matter [7,8], or living crystals [9,10]. Recently, active matter with nonreciprocal interactions (NRIs) has attracted a lot of attention, for which paradigmatic examples are the predator-prey relationship, visual perception [11,12], or flocking of unfriendly species [13–17]. The hallmark of NRIs is the emergence of a broad range of fascinating phenomena ranging from the spontaneous emergence of traveling waves [18,19] and chiral states [13] to odd viscosity [20], elasticity [21], and diffusivity [22,23].

In systems consisting of particles with only two-body interactions, nonreciprocity manifests itself by the violation of Newton's law "*actio* = *reactio*" such that the force or influence exerted by particle j on particle i, F_{ij}, is *not* equal to $-F_{ji}$. In complex systems with many species of particles, NRIs can be encoded in a nonsymmetric interaction matrix J_{ij}, as for instance, by nonsymmetric reaction rates for chemical mixtures or predator-prey systems. For complex systems consisting of a large number of species, this interaction matrix is frequently assumed to be random as in the context of neural networks [24–27], ecological communities [28–31], the immune system [32], coupled oscillators [33–36], and multispecies suspensions [37]. Random-field-type disorder, meaning heterogeneous environments instead of interactions, has been studied for the Vicsek model [38–42] and scalar active matter [43,44], but the impact of random nonreciprocal (NR) alignment interactions on flocking systems remains elusive.

Large ensembles of self-propelled particles may consist of many species with varying interspecies interactions, each of which can be aligning for friendly species or antialigning for unfriendly species [45]. In the simplest case of only two species, NRI gives rise to run-and-chase states, a traveling wave in which one species follows the other, and chiral states, in which all particles perform a coherent rotation [13–15,17], in addition to the still possible flocking state, in which all particles move collectively in the same direction. Whether these collective phenomena can survive in the presence of NRIs in a multispecies system is the question that we will address in this paper. Under which circumstances can flocking still occur or are chiral states still possible? If global order is destroyed, could local order in the form of microflocks or cliques occur? As a first step to shed light into these problems, we consider here a Vicsek-like model with random NRIs and tunable alignment bias between the individual particles. This setting includes two different types of scenarios: (1) A group of flocking animals of the same species is comprised of individuals with a common alignment bias but assigns NR corrections to the directional information received from other individuals, corresponding to weak NR randomness, and (2) a multispecies ensemble of self-propelled particles, in which each particle belongs to a different species and has its own NR alignment/antialignment rules with each of the other particles, corresponding to strong NR randomness. We will show that both scenarios bear the potential for collective phenomena absent in the conventional one- or two-species flocking models.

*Contact author: heiko.rieger@uni-saarland.de

The paper is organized as follows: In the next section, we define the model for which we first analyze the infinite-range limit in the third section. Then, in the fourth section we discuss finite-range interactions and discuss our results in the last section.

Model. We consider N self-propelled particles or agents i, characterized by a position $\mathbf{r}_i(t) \in L^d$ in a d-dimensional cube of lateral size L ($d = 2$ in this paper, p.b.c.) and a movement direction $\theta_i(t) \in [0, 2\pi]$. Their mutual tendency to move in the same direction as friendly neighbors (alignment) or to move in the opposite direction as unfriendly neighbors (antialignment) is described by a (noiseless) Vicsek-like model [5,46] defined by the equations of motion

$$\dot{\mathbf{r}}_i(t) = v_0\,(\cos(\theta_i(t)), \sin(\theta_i(t))), \tag{1}$$

$$\dot{\theta}_i(t) = -\sum_{j\in\mathcal{N}_i}\left(\frac{J_{ij}}{|\mathcal{N}_i|^\alpha} + \frac{J_0}{|\mathcal{N}_i|}\right)\sin(\theta_i(t) - \theta_j(t)). \tag{2}$$

The alignment/antialignment interactions consist of an alignment bias $J_0 \geqslant 0$ and of a random part J_{ij}, which can be aligning $J_{ij} > 0$ or antialigning $J_{ij} < 0$. The J_{ij} are Gaussian random variables with $\overline{J_{ij}} = 0$, $\overline{J_{ij}^2} = J^2$, and $\overline{J_{ij}J_{ji}} = \lambda J^2$, where $\lambda \in [-1, 1]$ controls the degree of nonreciprocity. Concretely, each interaction pair (J_{ij}, J_{ji}) is drawn from a bivariate Gaussian distribution

$$P(J_{ij}, J_{ji}) = \frac{1}{2\pi J^2\sqrt{1-\lambda^2}}\exp\left[-\frac{J_{ij}^2 - 2\lambda J_{ij}J_{ji} + J_{ji}^2}{2J^2(1-\lambda^2)}\right]. \tag{3}$$

In the limit $\lambda = \pm 1$, $P(J_{ij}, J_{ji})$ becomes singular: For $\lambda = 1$, the interaction pair is strictly reciprocal ($J_{ij} = J_{ji}$), while for $\lambda = -1$ it is antisymmetric ($J_{ij} = -J_{ji}$). We set $J = 1$ and measure J_0 and time t in units of J. v_0 denotes the self-propulsion speed.

$\mathcal{N}_i$ is the neighborhood of particle i, comprising all particles j in a distance smaller than R, and $|\mathcal{N}_i|$ is the number of particles in this neighborhood. In the case of infinite-range interactions ($R \to \infty$), $|\mathcal{N}_i| = N$. The exponent $\alpha \in \{1/2, 1\}$ denotes different scalings of the interaction strengths: $\alpha = 1/2$ has to be chosen in order to obtain a nontrivial mean-field limit $N, R \to \infty$, $\alpha = 1$ is legitimate for any finite N and weights bias and randomness similarly. Coherent motion of a flock is indicated by the order parameter $\vec{m}(t) = 1/N\sum_i(\cos\theta_i(t), \sin\theta_i(t)) = m(t) \times (\cos\psi(t), \sin\psi(t))$, and flocking occurs when $m(t) > 0$.

Infinite-range limit: Phase behaviors. For $R \to \infty$, the particle-particle interactions are independent of the particle positions $\mathbf{r}_i$ and the angles θ_i evolve according to Eq. (2) with $|\mathcal{N}_i| = N$. Flocking occurs when J_0 is larger than a critical alignment bias, which for $\alpha = 1$ decreases with N as $J_{0,c}/\sqrt{N}$ [Fig. 1(a)], with $J_{0,c} = 1.1$, implying that flocking emerges for any $J_0 > 0$ in the limit $N \to \infty$.

In contrast, for $\alpha = 1/2$, Eq. (2) reduces in the limit $N \to \infty$ to a self-consistent stochastic single-particle dynamics or dynamical mean-field theory (DMFT) [25,26,33,35,49]. For $\lambda = 0$, this DMFT is given by

$$\dot{\theta}(t) = (\varphi_y(t) + J_0 m_y(t))\cos\theta(t) - (\varphi_x(t) + J_0 m_x(t))\sin\theta(t), \tag{4}$$

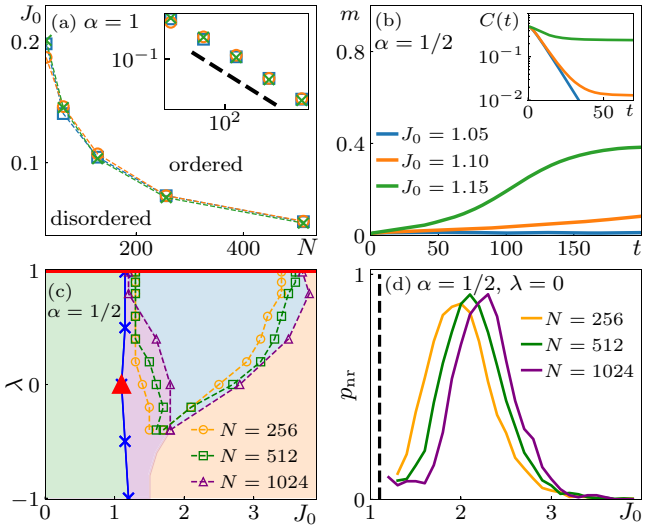

FIG. 1. (a) Infinite-range phase diagram for $\alpha = 1$ and $\lambda = -0.5$ (circle), 0 (square), and 0.5 (cross). Inset: Log-log plot of the phase diagram. Black dashed line indicates $J_0 \sim N^{-1/2}$. (b) Order parameter $m(t)$ for different J_0 at $\lambda = 0$ obtained by solving the DMFT equation (4). The critical point is $J_{0,c} \approx 1.1$. Inset: Correlation function $C(t)$ for the same values of J_0 as in the main figure. (c) J_0-λ phase diagram for $\alpha = 1/2$. Green: disordered phase; purple: flocking with relaxational dynamics [cf. Fig. 2(a)]; blue: flocking region with nonrelaxational dynamics [cf. Figs. 2(b)–2(d) and panel (d)]. Note that this region shrinks with increasing N (see text). Orange: static flocking. The blue line indicates the disorder-flocking phase boundary [47]) and the red line represents the spin glass region at $\lambda = 1$. The red triangle locates the critical point from DMFT at $\lambda = 0$. (d) Fraction of disorder realizations displaying nonrelaxational dynamics $p_{\rm nr}$ as a function of J_0 (at $\lambda = 0$). The black dashed line indicates the critical point from DMFT. $p_{\rm nr} > 0.15$ defines the blue region in panel (d).

where $\varphi_a(t)$ for $a = x, y$ is Gaussian colored noise with zero mean and correlations $\langle\varphi_a(t)\varphi_a(t')\rangle = C_{ab}(t, t')$, which are self-consistently given by the dynamics of θ via $C_{xx}(t, t') = \langle\cos\theta(t)\cos\theta(t')\rangle_\varphi$, $C_{yy}(t, t') = \langle\sin\theta(t)\sin\theta(t')\rangle_\varphi$, etc. and the magnetization $(m_x(t), m_y(t)) = (\langle\cos\theta(t)\rangle_\varphi, \langle\sin\theta(t)\rangle_\varphi)$. By solving Eq. (4) numerically [50], we determine for $\lambda = 0$ the time dependence of the order parameter $m(t)$ [Fig. 1(b)] and the stationary autocorrelation function $C(t) = \lim_{t_0\to\infty} C(t + t_0, t_0)$ [Fig. 1(b), inset], which approach exponentially fast either zero in the disordered phase or $m_s > 0$ and m_s^2, respectively, in the flocking phase. These results also confirm the flocking transition to be at $J_{0,c} = 1.1$ for $\lambda = 0$. The complete J_0-λ phase diagram obtained by numerically integrating Eq. (1) and performing finite-size scaling [47] is shown in Fig. 1(c).

Infinite-range limit: Nonrelaxational dynamics for finite N. In contrast to the purely relaxational behavior of the DMFT ($N \to \infty$) of uncorrelated randomness ($\lambda = 0$), the dynamics of a finite system ($N < \infty$) is much more interesting and can exhibit various nonrelaxational dynamics such as oscillations, rotations, and vibrating oscillations as shown in Figs. 2(b)–2(d) and Movie S2 of the Supplemental Material [47]. These attractors emerge in the whole blue region of Fig. 1(c) within the flocking phase and persist up to, but not including, $\lambda = 1$.

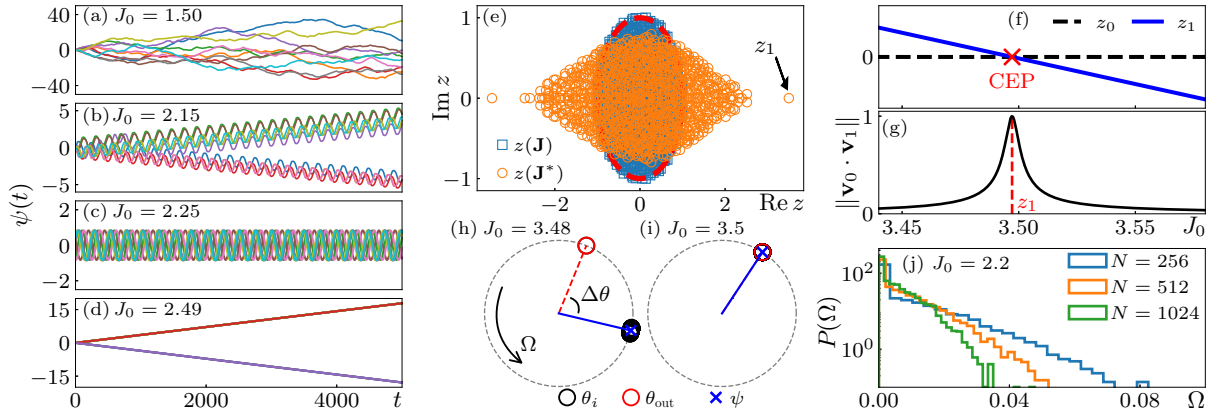

FIG. 2. Emergence of nonrelaxational dynamics for finite N with infinite-range interactions. (a)–(d) Time evolution of magnetization phase $\psi(t)$ for a single realization of interaction matrix $[\mathbf{J}]_{ij} = J_{ij}/\sqrt{N}$ with $N = 1024$ and $\lambda = 0$: (a) flocking with diffusive $\psi(t)$, (b) vibrating oscillation, (c) oscillation, and (d) rotation (see Movie S2 of the Supplemental Material [47]. Each line in panels (a)–(d) represents trajectories of $\psi(t)$ starting from different initial conditions. (e) Eigenvalue spectrum of the same interaction matrix $\mathbf{J}$ as in panels (a)–(d) and the corresponding linearized matrix $\mathbf{J}^*$, for $J_0 = 0$. The red dashed line indicates the circular law for $\lambda = 0$ [48] and z_1 depicts the leading eigenvalue of $\mathbf{J}^*$, which locates the critical exceptional point (CEP): (f) Decreasing $J_0 > z_1$ shifts the spectrum to the right, and z_1 hits zero at the CEP ($z_1 \approx 3.497$) and (g) overlap between eigenvector $\mathbf{v}_1$ associated with z_1 and the Goldstone mode $\mathbf{v}_0$ reaches 1, indicating two eigenvectors coalesce. (h), (i) Steady-state angle configuration near the CEP. (h) For $J_0 = 3.48 < z_1$, the outlier component θ_{out} is separated from the others with constant angle difference $\Delta\theta = \theta_{\text{out}} - \psi$ and drives global chiral motion with constant angular velocity Ω. (i) For $J_0 = 3.50 > z_1$, all angles are perfectly aligned. (j) Probability distribution of the time-averaged angular velocity $P(\Omega)$ in the steady state for fixed $J_0 = 2.2$ and varying N.

At $\lambda = 1$, Eq. (2) predicts a zero-temperature spin glass phase in which the angles θ_i relax into a local energy minimum of the underlying XY Hamiltonian and freeze. We analyze the nonrelaxational behavior for finite N by linearizing the equation of motion by $\theta_i = \psi + \delta_i$ for $J_0 \gg J_{0,c}$. The linearized equation of motion is then

$$\dot{\vec{\delta}} = \mathbf{J}^* \vec{\delta}, \tag{5}$$

where $[\mathbf{J}^*]_{ij} = J_{ij}/\sqrt{N} + J_0/N$ for $i \neq j$ and $[\mathbf{J}^*]_{ii} = -\sum_{j\neq i}[\mathbf{J}^*]_{ij}$. While the eigenvalue spectrum of the original interaction matrix $\mathbf{J}$ follows the circular law [48], that of the linearized matrix $\mathbf{J}^*$ at $J_0 = 0$ is deformed due to rotational symmetry $\sum_j [\mathbf{J}^*]_{ij} = 0$ [Fig. 2(e)]. The ferromagnetic bias $J_0 > 0$ only shifts the entire eigenvalue spectrum of $\mathbf{J}^*$ by $-J_0$ along the Re z axis, except for the Goldstone mode $\mathbf{v}_0 = N^{-1/2}(1, \ldots, 1)^T$, whose eigenvalue remains at zero [47]. Therefore, for $J_0 > z_1$, where z_1 denotes the leading eigenvalue of $\mathbf{J}^*$, all eigenmodes decay to zero, and the system settles into a static ordered phase with perfect alignment $\theta_i = \psi$ [Fig. 2(i)].

As J_0 decreases and approaches z_1, the leading eigenvalue z_1 hits the Goldstone mode at zero [Fig. 2(f)], and the associated eigenvector $\mathbf{v}_1$ coalesces with $\mathbf{v}_0$ [Fig. 2(g)]. This is the hallmark of a CEP [52–54] beyond which chiral motion emerges. At the CEP, all angles still stay close and begin to rotate collectively. As J_0 decreases further, one "outlier" θ_{out} gradually deviates from the other angles but continues to rotate with them [Fig. 2(h)]. As soon as the angle difference reaches π, the chiral motion stops and the static ordered state is restored [47] and remains stable until a second instability arises. The nature of the second instability can be a Hopf bifurcation or again a critical exceptional point, depending on eigenvalue spectrum. In the bulk spectrum, where multiple instabilities contribute, we observe nonrelaxational behaviors shown in Figs. 2(b)–2(d) at sufficiently high J_0 [Fig. 1(d)]. Notably, the chiral states also exist for finite-range interactions if all particles are located within a small circle and have sufficiently small self-propulsion speed v_0 [47].

To render this complex finite-N behavior consistent with the mean-field predictions ($N \to \infty$), we analyzed the finite-size behavior of the probability distribution of the stationary angular frequency $\Omega = \langle \dot{\psi}(t) \rangle$, where $\langle \cdots \rangle$ denotes a time average. Figure 2(j) shows that the support of $P(\Omega)$ shrinks with increasing system size N, which implies that any rotational motion of the order parameter becomes on average slower with increasing system size and ceases in the limit $N \to \infty$. We note that even for large but finite system sizes still slow rotations exist, which renders a precise extrapolation of observables to infinite system size by integrating Eq. (2) computationally unfeasible. Nevertheless, the proper $N \to \infty$ limit is given by the solution of Eq. (4).

Finite interaction range: Phase diagram. In the case of a finite interaction range R, we integrate Eqs. (1) and (2) using the Euler method with time step $dt = 0.05$ and propulsion speed $v_0 = 0.5$. We set $R = 1$ and discuss here only uncorrelated randomness $\lambda = 0$. For $\alpha = 1$, flocking already occurs for small alignment bias $J_0 \ll J(= 1)$, which decreases with increasing density, $\rho = N/L^2$, as shown in Fig. 3(a), reminiscent of the decrease of $J_{0,c}(N)$ with N for the infinite-range case. In the flocking phase, except for small ρ, the system eventually evolves into a single dense cluster in which all particles are tightly packed and move coherently [inset of Fig. 3(a)]. This single-cluster phase emerges via nucleation: Once a denser cluster forms, the contribution of the alignment bias to the

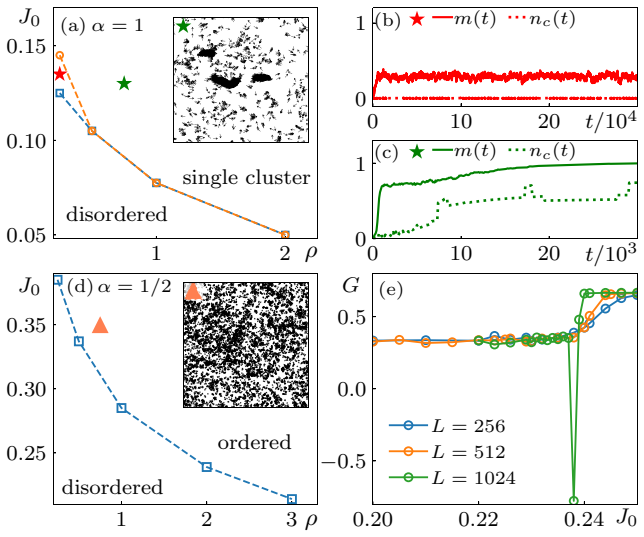

FIG. 3. Finite-range interactions ($R = 1$, $\lambda = 0$): (a) Phase diagram for $\alpha = 1$. Region between the disordered and the single-cluster phase indicates long-range order $m > 0$ without condensation. Inset: Configuration snapshot ($L = 1024$) of growing clusters in the single-cluster region at the point marked with green star in panel (a). (b), (c) Time evolution of magnetization $m(t)$ and the relative size of the largest cluster $n_c(t)$ at the red and green points marked in panel (a). (d) As in panel (a) for $\alpha = 1/2$. Inset: Configuration snapshot in the ordered region at the orange triangle in panel (c). (e) Binder cumulant $G = 1 - \langle m^4 \rangle / (3\langle m^2 \rangle^2)$ at the transition ($\rho = 2$).

interactions dominates over the random contribution due to the $\alpha = 1$ scaling, such that the cluster eventually absorbs all particles [Fig. 3(c)].

For $\alpha = 1/2$, the critical alignment bias $J_{0,c}$ also decreases with increasing density ρ, as shown in Fig. 3(d). In both cases, for $\alpha = 1/2$ and $\alpha = 1$, the transition from the disordered phase to the flocking phase is discontinuous [Fig. 3(e)], reminiscent of the Vicsek model [46,55]. In contrast to the latter, when crossing the transition line in Fig. 3(d), for instance, by increasing the density ρ, spontaneously global polar order emerges without an intermediate band formation. As we increase J_0 further, we also find a transition to a single-cluster phase (see Fig. S4 of the Supplemental Material [47]). Here, the single-cluster phase arises due to coarsening, where small clusters move ballistically and merge into a larger cluster upon collision as in the conventional Vicsek model at very low noise [56].

Finite interaction range: Clique formation. Both disordered and ordered phases in the low-density regime are characterized by clique formation, where transient clusters of coherently moving particles emerge and disintegrate dynamically even in the absence of a ferromagnetic bias $J_0 = 0$. To analyze these cliques, we construct interaction networks based on the distance between particles at successive simulation times and track the evolution of their connected components [51] [Fig. 4(a)]. Among the connected components that persist over time, we define a "clique" $\mathcal{C}(n, \tau)$ as a set of particles in a connected component with size n and lifetime τ, restricted to those with $n \geqslant 5$ and $\tau \geqslant 10$ [Fig. 4(c)]. Figure 4(b) represents an example time series for a specific particle, illustrating that only a small subset of its interacting neighbors actually form cliques with it. Figure 4(d) shows $P(n, \tau)$, the probability that a particle belongs to $\mathcal{C}(n, \tau)$, averaged over time and disorder. Both $P(n)$ and $P(\tau)$ exhibit exponential tail [Figs. 4(e) and 4(g)] and the characteristic clique size n^* and lifetime τ^* are extracted from exponential fits [Figs. 4(f) and 4(h)]. Notably, here the lifetime τ of medium- and small-size cliques is actually sufficiently long for them to traverse half of the system.

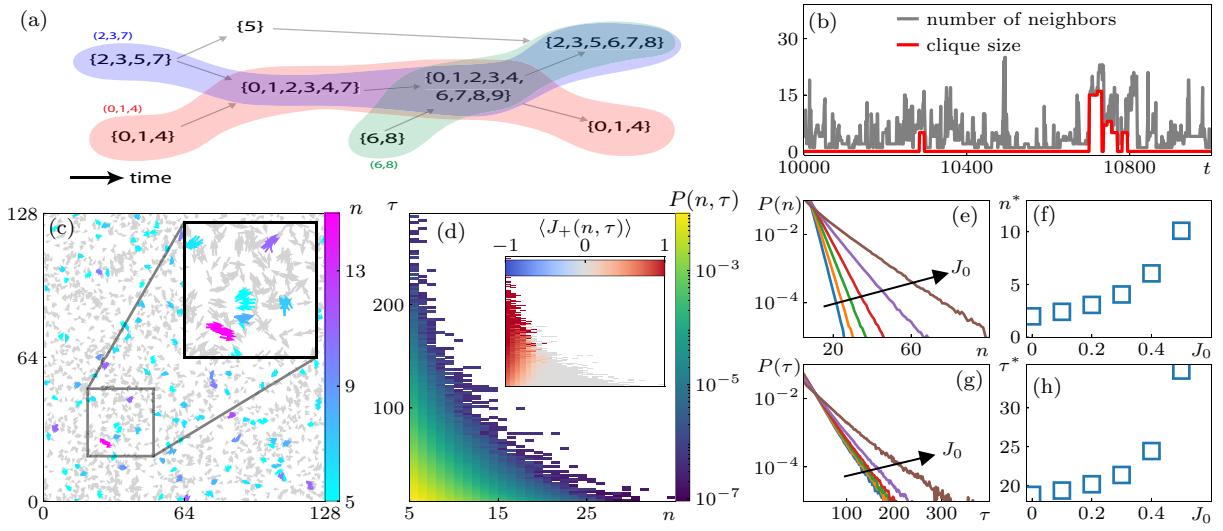

FIG. 4. Clique formation for finite-range interactions ($R = 1$, $\lambda = 0$, $\alpha = 1/2$, $\rho = 0.25$). (a) Schematic diagram of the clique detecting algorithm [51]. Each set $\{\cdots\}$ represents connected components and arrow depicts particle flows between connected components at different times. The colored regions indicate three potential cliques: {2, 3, 7} (blue), {0, 1, 4} (red), and {6, 8} (green). (b) Time evolution of the number of interacting neighbors of a specific particle and the size of the largest clique containing it. (c) Snapshot of a particle configuration for $J_0 = 0$. Cliques are represented with colors according to their size. Inset: Enlarged snapshot of the region indicated by the gray square. (d) $P(n, \tau)$ at $J_0 = 0$ averaged over many disorder realizations. Inset: $\langle J_+(n, \tau)\rangle$ at the same parameters as panel (d). (e), (f) $P(n)$ for different J_0 values and its characteristic cluster size n^*. (g), (h) $P(\tau)$ for different J_0 values and its characteristic lifetime τ^*.

The formation of a clique is driven by the self-assembly of particles with predominantly mutual aligning interactions $\langle J_+(n,\tau)\rangle > 0$, where $J_+(n,\tau)$ is an average of $2J_0 + J_{ij} + J_{ji}$ over the members i, j of a clique, as shown in the inset of Fig. 4(d). Cliques disintegrate when they collide with other strongly interacting particles or cliques [47]. When compared with clusters emerging in the disordered phase of the conventional Vicsek model with homogeneous alignment interactions one notes that in the latter clusters are typically larger but have shorter lifetimes.

Discussion. We have shown that flocking can occur in an ensemble of self-propelled particles with a random mixture of nonreciprocal aligning and antialigning. Within the ordered phase, for sufficiently strong alignment bias, spurious chiral states emerge in finite systems with infinite-range interaction, separated from conventional flocking by exceptional points or Hopf bifurcations. Those states disappear in the infinite system size limit, where purely relaxational dynamics toward global flocking persists. For finite interaction range, coherently moving cliques emerge, in which a small group of particles self-organize transiently, even in the absence of a global alignment bias in the interactions: Equipped with random and fully nonreciprocal ($\lambda = 0$) interactions J_{ij}, particles with J_{ij} and J_{ji} positive (aligning) find each other and move for some time together until they collide with other groups. It should be noted that this clique formation is different from conventional cluster formation, in which particles can join and leave clusters: A clique is defined as a specific group of particles that stays together until the clique dissolves [57].

In a forthcoming publication [58], we will discuss the robustness of these phenomena in the presence of noise or the introduction of the Vicsek update rules for directional changes. Our preliminary results show that the (λ, J_0, nonreciprocity/alignment bias) phase diagrams that we reported are robust with respect to the introduction of weak noise as well as Vicsek update rules. Also, the chiral states of finite systems in the ordered phase of the infinite-range limit are stable against weak noise as well as the clique formation for finite interaction range. Stronger noise will, however, have an impact. Also, the variation of the degree of nonreciprocity bears interesting aspects as an enhanced tendency to order for $\lambda \to 1$ and an emerging spin glass phase at $\lambda = 1$.

Our results may serve as a starting point for the study of multispecies flocking models with nonrandom but complex nonreciprocal interspecies interactions in the following sense: As nonreciprocal interactions are used to generate temporal sequences of patterns in neural network models [24] or for dynamical control of self-assembled immobile structures and transitions between them [59], we expect that programmable nonreciprocal interactions in flocking models as the one analyzed here could be a tool to create mobile "shape shifters" made of self-propelled particles that arrange in a predetermined temporal sequence of patterns with varying shapes. It would be worthwhile to examine this vision in future work.

Note added. When this paper was completed, we became aware of a recent work in which a similar phenomenon has been observed in a flocking model with fully reciprocal ($\lambda = 1$), spin-glass-like couplings and with the scaling $\alpha = 1$, which, in contrast to the case $\lambda = 0$ that we analyzed, shows global flocking (see Ref. [57]).

Data availability. The data that support the findings of this article are not publicly available upon publication because it is not technically feasible and/or the cost of preparing, depositing, and hosting the data would be prohibitive within the terms of this research project. The data are available from the authors upon reasonable request.

[1] M. C. Marchetti, J. F. Joanny, S. Ramaswamy, T. B. Liverpool, J. Prost, M. Rao, and R. A. Simha, Hydrodynamics of soft active matter, Rev. Mod. Phys. **85**, 1143 (2013).

[2] S. Ramaswamy, The mechanics and statistics of active matter, Annu. Rev. Condens. Matter Phys. **1**, 323 (2010).

[3] C. Bechinger, R. Di Leonardo, H. Löwen, C. Reichhardt, G. Volpe, and G. Volpe, Active particles in complex and crowded environments, Rev. Mod. Phys. **88**, 045006 (2016).

[4] M. R. Shaebani, A. Wysocki, R. G. Winkler, G. Gompper, and H. Rieger, Computational models for active matter, Nat. Rev. Phys. **2**, 181 (2020).

[5] T. Vicsek, A. Czirók, E. Ben-Jacob, I. Cohen, and O. Shochet, Novel type of phase transition in a system of self-driven particles, Phys. Rev. Lett. **75**, 1226 (1995).

[6] M. E. Cates and J. Tailleur, Motility-induced phase separation, Annu. Rev. Condens. Matter Phys. **6**, 219 (2015).

[7] A. Bricard, J.-B. Caussin, N. Desreumaux, O. Dauchot, and D. Bartolo, Emergence of macroscopic directed motion in populations of motile colloids, Nature (London) **503**, 95 (2013).

[8] V. Schaller, C. Weber, C. Semmrich, E. Frey, and A. R. Bausch, Polar patterns of driven filaments, Nature (London) **467**, 73 (2010).

[9] I. Theurkauff, C. Cottin-Bizonne, J. Palacci, C. Ybert, and L. Bocquet, Dynamic clustering in active colloidal suspensions with chemical signaling, Phys. Rev. Lett. **108**, 268303 (2012).

[10] J. Palacci, S. Sacanna, A. P. Steinberg, D. J. Pine, and P. M. Chaikin, Living crystals of light-activated colloidal surfers, Science **339**, 936 (2013).

[11] F. A. Lavergne, H. Wendehenne, T. Bäuerle, and C. Bechinger, Group formation and cohesion of active particles with visual perception-dependent motility, Science **364**, 70 (2019).

[12] L. Barberis and F. Peruani, Large-scale patterns in a minimal cognitive flocking model: Incidental leaders, nematic patterns, and aggregates, Phys. Rev. Lett. **117**, 248001 (2016).

[13] M. Fruchart, R. Hanai, P. B. Littlewood, and V. Vitelli, Nonreciprocal phase transitions, Nature (London) **592**, 363 (2021).

[14] K. L. Kreienkamp and S. H. L. Klapp, Nonreciprocal alignment induces asymmetric clustering in active mixtures, Phys. Rev. Lett. **133**, 258303 (2024).

[15] M. Mangeat, S. Chatterjee, J. D. Noh, and H. Rieger, Emergent complex phases in a discrete flocking model with reciprocal and non-reciprocal interactions, Commun. Phys. **8**, 186 (2025).

[16] Y. Avni, M. Fruchart, D. Martin, D. Seara, and V. Vitelli, Nonreciprocal Ising model, Phys. Rev. Lett. **134**, 117103 (2025).

[17] Y. Avni, M. Fruchart, D. Martin, D. Seara, and V. Vitelli, Dynamical phase transitions in the nonreciprocal Ising model, Phys. Rev. E **111**, 034124 (2025).

[18] Z. You, A. Baskaran, and M. C. Marchetti, Nonreciprocity as a generic route to traveling states, Proc. Natl. Acad. Sci. USA **117**, 19767 (2020).
[19] F. Brauns and M. C. Marchetti, Nonreciprocal pattern formation of conserved fields, Phys. Rev. X **14**, 021014 (2024).
[20] D. Banerjee, A. Souslov, A. G. Abanov, and V. Vitelli, Odd viscosity in chiral active fluids, Nat. Commun. **8**, 1573 (2017).
[21] C. Scheibner, A. Souslov, D. Banerjee, P. Surówka, W. T. M. Irvine, and V. Vitelli, Odd elasticity, Nat. Phys. **16**, 475 (2020).
[22] C. Hargus, J. M. Epstein, and K. K. Mandadapu, Odd diffusivity of chiral random motion, Phys. Rev. Lett. **127**, 178001 (2021).
[23] E. Kalz, H. D. Vuijk, I. Abdoli, J.-U. Sommer, H. Löwen, and A. Sharma, Collisions enhance self-diffusion in odd-diffusive systems, Phys. Rev. Lett. **129**, 090601 (2022).
[24] H. Sompolinsky and I. Kanter, Temporal association in asymmetric neural networks, Phys. Rev. Lett. **57**, 2861 (1986).
[25] A. Crisanti and H. Sompolinsky, Dynamics of spin systems with randomly asymmetric bonds: Langevin dynamics and a spherical model, Phys. Rev. A **36**, 4922 (1987).
[26] H. Rieger, M. Schreckenberg, and J. Zittartz, Glauber dynamics of neural network models, J. Phys. A: Math. Gen. **21**, L263 (1988).
[27] H. Sompolinsky, A. Crisanti, and H. J. Sommers, Chaos in random neural networks, Phys. Rev. Lett. **61**, 259 (1988).
[28] H. Rieger, Solvable model of a complex ecosystem with randomly interacting species, J. Phys. A: Math. Gen. **22**, 3447 (1989).
[29] A. Altieri, F. Roy, C. Cammarota, and G. Biroli, Properties of equilibria and glassy phases of the random Lotka-Volterra model with demographic noise, Phys. Rev. Lett. **126**, 258301 (2021).
[30] V. Ros, F. Roy, G. Biroli, G. Bunin, and A. M. Turner, Generalized Lotka-Volterra equations with random, nonreciprocal interactions: The typical number of equilibria, Phys. Rev. Lett. **130**, 257401 (2023).
[31] G. Garcia Lorenzana, A. Altieri, and G. Biroli, Interactions and migration rescuing ecological diversity, Phys. Rev. X Life **2**, 013014 (2024).
[32] G. Parisi, A simple model for the immune network, Proc. Natl. Acad. Sci. USA **87**, 429 (1990).
[33] J. C. Stiller and G. Radons, Dynamics of nonlinear oscillators with random interactions, Phys. Rev. E **58**, 1789 (1998).
[34] A. Prüser, S. Rosmej, and A. Engel, Nature of the volcano transition in the fully disordered Kuramoto model, Phys. Rev. Lett. **132**, 187201 (2024).
[35] A. Prüser and A. Engel, Role of coupling asymmetry in the fully disordered Kuramoto model, Phys. Rev. E **110**, 064214 (2024).
[36] R. Hanai, Nonreciprocal frustration: Time crystalline order-by-disorder phenomenon and a spin-glass-like state, Phys. Rev. X **14**, 011029 (2024).
[37] L. Parkavousi, N. Rana, R. Golestanian, and S. Saha, Enhanced stability and chaotic condensates in multispecies nonreciprocal mixtures, Phys. Rev. Lett. **134**, 148301 (2025).
[38] Y. Duan, B. Mahault, Y.-q. Ma, X.-q. Shi, and H. Chaté, Breakdown of ergodicity and self-averaging in polar flocks with quenched disorder, Phys. Rev. Lett. **126**, 178001 (2021).
[39] O. Chepizhko, E. G. Altmann, and F. Peruani, Optimal noise maximizes collective motion in heterogeneous media, Phys. Rev. Lett. **110**, 238101 (2013).
[40] A. Chardac, S. Shankar, M. C. Marchetti, and D. Bartolo, Emergence of dynamic vortex glasses in disordered polar active fluids, Proc. Natl. Acad. Sci. USA **118**, e2018218118 (2021).
[41] A. Morin, N. Desreumaux, J.-B. Caussin, and D. Bartolo, Distortion and destruction of colloidal flocks in disordered environments, Nat. Phys. **13**, 63 (2016).
[42] J. Codina, B. Mahault, H. Chaté, J. Dobnikar, I. Pagonabarraga, and X.-q. Shi, Small obstacle in a large polar flock, Phys. Rev. Lett. **128**, 218001 (2022).
[43] S. Ro, Y. Kafri, M. Kardar, and J. Tailleur, Disorder-induced long-ranged correlations in scalar active matter, Phys. Rev. Lett. **126**, 048003 (2021).
[44] Y. Ben Dor, S. Ro, Y. Kafri, M. Kardar, and J. Tailleur, Disordered boundaries destroy bulk phase separation in scalar active matter, Phys. Rev. E **105**, 044603 (2022).
[45] S. Chatterjee, M. Mangeat, C.-U. Woo, H. Rieger, and J. D. Noh, Flocking of two unfriendly species: The two-species Vicsek model, Phys. Rev. E **107**, 024607 (2023).
[46] G. Grégoire and H. Chaté, Onset of collective and cohesive motion, Phys. Rev. Lett. **92**, 025702 (2004).
[47] See Supplemental Material at http://link.aps.org/supplemental/10.1103/y26b-qfym for additional analysis of finite-size scaling at the critical point, discussion of chiral states in infinite- and finite-range interactions, emergence of single-cluster phase, and description of supplemental movies.
[48] H. J. Sommers, A. Crisanti, H. Sompolinsky, and Y. Stein, Spectrum of large random asymmetric matrices, Phys. Rev. Lett. **60**, 1895 (1988).
[49] G. G. Lorenzana, A. Altieri, G. Biroli, M. Fruchart, and V. Vitelli, Non-reciprocal spin-glass transition and aging, Phys. Rev. Lett. **135**, 187402 (2025).
[50] F. Roy, G. Biroli, G. Bunin, and C. Cammarota, Numerical implementation of dynamical mean field theory for disordered systems: Application to the Lotka–Volterra model of ecosystems, J. Phys. A: Math. Theor. **52**, 484001 (2019).
[51] K. Buchin, M. Buchin, M. V. Kreveld, B. Speckmann, and F. Staals, Trajectory grouping structure, J. Comput. Geom. **6**, 75 (2015).
[52] R. Hanai and P. B. Littlewood, Critical fluctuations at a many-body exceptional point, Phys. Rev. Res. **2**, 033018 (2020).
[53] C. P. Zelle, R. Daviet, A. Rosch, and S. Diehl, Universal phenomenology at critical exceptional points of nonequilibrium O(N) models, Phys. Rev. X **14**, 021052 (2024).
[54] T. Suchanek, K. Kroy, and S. A. M. Loos, Time-reversal and parity-time symmetry breaking in non-Hermitian field theories, Phys. Rev. E **108**, 064123 (2023).
[55] H. Chaté, F. Ginelli, G. Grégoire, and F. Raynaud, Collective motion of self-propelled particles interacting without cohesion, Phys. Rev. E **77**, 046113 (2008).
[56] L. Barberis, Emergence of a single cluster in Vicsek's model at very low noise, Phys. Rev. E **98**, 032607 (2018).
[57] E. Lardet, R. Voituriez, S. Grigolon, and T. Bertrand, Disordered yet directed: The emergence of polar flocks with disordered interactions, arXiv:2409.10768.
[58] J. Choi and H. Rieger (unpublished).
[59] S. Osat and R. Golestanian, Non-reciprocal multifarious self-organization, Nat. Nanotechnol. **18**, 79 (2022).